2016 American Control Conference (ACC)
Boston Marriott Copley Place
July 6-8, 2016. Boston, MA, USA

Estimation of feedback gains and delays in connected vehicle systems

Jin I. Ge and Gábor Orosz

Abstract— **In this paper, we present different parameter estimation methods that may be used to identify the dynamics of human-driven vehicles in connected vehicle systems. By exploiting the information received via wireless vehicle-to-vehicle communication from two consecutive vehicles ahead, the estimation algorithms identify the driver reaction time and feedback gains simultaneously. We compare the algorithms in terms of convergence rate and estimation accuracy, and present a systematic way to improve both performance measures. The estimated parameters can then be used in connected cruise control algorithms that incorporate the transmitted signals in a vehicle's longitudinal motion control.**

I. Introduction

Various advanced driver assistance systems have been proposed over the past decades in order to improve road transportation. Specifically, adaptive cruise control (ACC) uses onboard sensors such as radar/lidar to obtain motion information faster and more accurately than human drivers, and provides more adequate commands for the longitudinal motion control [1]. With the availability of affordable wireless communication devices, connected cruise control (CCC) has been proposed [2] to exploit motion information of vehicles over a longer range, so that undesired acceleration/deceleration of the CCC vehicle can be further suppressed. This may lead to higher road efficiency, less fuel consumption and improved safety in connected vehicle systems.

Existing research on CCC design generally assumes a priori knowledge on the dynamics of preceding vehicles whose signals are used in the CCC controller [3], [4]. Such an assumption may not hold, when the ad-hoc wireless communication allows vehicles to join and leave the connected vehicle system. Thus, it is necessary to consider online identification of car-following dynamics of preceding vehicles [5]. We choose the parametric model to be a car-following model with driver reaction time, as it has been found to be able to describe a wide range of driving behaviors. The driver reaction time is included, because it has been shown that the large driver reaction time has a significant influence on the performance of connected vehicle systems which include human-driven, ACC, and CCC vehicles [6]. Although in this paper we assume that all non-CCC vehicles are human-driven, the identification algorithms are able to deal with ACC vehicles, as the latter can also be described by car-following models but with smaller reaction time.

Jin I. Ge and Gábor Orosz are with the Department of Mechanical Engineering, University of Michigan, Ann Arbor, Michigan 48109, USA gejin@umich.edu, orosz@umich.edu

This work was supported by the National Science Foundation (award number 1351456)

The methodology for parameter identification in systems without time delay has been well developed over the years. Many adaptive laws were designed based on Lyapunov technique [7]. While there exist some results concerning parameter estimation in time delay systems [8], [9], estimating the delay time and feedback gains simultaneously is still a challenging problem [10], [11]. Such estimators typically lead to systems with state-dependent delay, where it is difficult to design the convergence rate and region of attraction.

In this paper, we present three methods for simultaneous identification of the feedback gains and delay. The first (and most straightforward) method converts the problem of estimating delay time into estimating feedback gains. To overcome the large computational need and slow convergence rate of the first method, we propose the second method which explicitly estimates the delay time parallel to the feedback gains. The third method is proposed to improve the convergence rate of the second method by introducing additional nonlinearities. Numerical simulations are used to compare the performance of the three methods.

II. Connected vehicle system setup

We consider the configuration in Fig. 1(a) where a group of vehicles travel on a single lane. We assume that vehicle 1 receives the motion information of $N-1$ vehicles ahead through wireless vehicle-to-vehicle (V2V) communication. By using signals from two consecutive vehicles ahead (vehicles i and $i+1$), vehicle 1 is able to identify the dynamics of vehicle i and thus uses motion information of vehicle i for its longitudinal control. In this way, vehicle 1 can include feedback terms on the headway and velocity signals from multiple vehicles ahead, which we refer as connected cruise control [6], [12].

A. Nonlinear car-following model

The non-CCC vehicles ($i = 2, \ldots, N-1$) are assumed to be human-driven and their dynamics is described by the conventional car-following model

$$\begin{aligned} \dot{h}_i(t) &= v_{i+1}(t) - v_i(t)\,, \\ \dot{v}_i(t) &= \alpha\big(V(h_i(t-\tau)) - v_i(t-\tau)\big) \\ &\quad + \beta\big(v_{i+1}(t-\tau) - v_i(t-\tau)\big)\,. \end{aligned} \tag{1}$$

Here the dot stands for differentiation with respect to time t, h_i denotes the headway, i.e., the bumper-to-bumper distance between vehicle i and its predecessor), and v_i denotes the velocity of vehicle i; see Fig. 1(a). According to (1) the acceleration of a non-CCC vehicle is determined by two terms: the difference between the headway-dependent desired

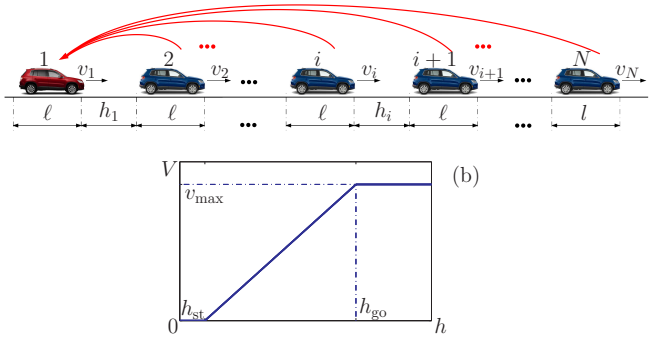

Fig. 1. (a): A string of N vehicles with a CCC vehicle at the tail receiving signals from human-driven vehicles ahead via wireless V2V communication. The red arrows denote information flow. The velocity of vehicle i is denoted by v_i. The bumper-to-bumper distance between vehicle i and vehicle $i+1$ is called the headway and denoted as h_i. The length of every vehicle is assumed to be l. (b): The range policy function defined by (2).

velocity and the actual velocity and the velocity difference between the vehicle and its predecessor. The gains α and β are used by the human drivers to correct velocity errors, and τ is the human reaction time.

The desired velocity is determined by a nonlinear range policy function

$$V(h) = \begin{cases} 0 & \text{if} \quad h \le h_{\rm st}\,, \\ v_{\max}\dfrac{h-h_{\rm st}}{h_{\rm go}-h_{\rm st}} & \text{if} \quad h_{\rm st} < h < h_{\rm go}\,, \\ v_{\max} & \text{if} \quad h \ge h_{\rm go}\,, \end{cases} \tag{2}$$

which is shown in Fig. 1(b). That is, the desired velocity is zero for small headways ($h \le h_{\rm st}$) and equal to the maximum speed $v_{\max}$ for large headways ($h \ge h_{\rm go}$). Between these, the desired velocity increases with the headway linearly. Many other range policies may be chosen, but the qualitative dynamics remain similar if the above characteristics are kept [13]. The model (1,2) is adapted from [13], [14] and can be obtained as a simplification of the physics-based model presented in [2].

Note that the model (1,2) does not describe dynamics in emergency situations. For the same reason, we do not consider feedback terms related with the motion of vehicles behind.

B. Linearization

We assume the dynamics of the connected vehicle system (1,2) to be in the vicinity of the uniform flow equilibrium where all vehicles travel with the same constant velocity and maintain the same constant headway, that is,

$$h_i(t) \equiv h^*\,, \quad v_i(t) \equiv v^* = V(h^*)\,, \tag{3}$$

for $i = 1, \dots, N$. Here the equilibrium velocity v^* is determined by the head vehicle in a vehicle string, while the equilibrium headway h^* can be calculated from the range policy (2).

We define the headway perturbations $\delta h_i(t) = h_i(t) - h^*$ and velocity perturbations $\delta v_i(t) = v_i(t) - v^*$, for $i = 1, \dots, N$, and linearize (1) about the equilibrium (3). This yields the linear delay differential equation

$$\begin{aligned} \delta\dot{h}_i(t) =\ & \delta v_{i+1}(t) - \delta v_i(t)\,, \\ \delta\dot{v}_i(t) =\ & -(\alpha+\beta)\delta v_i(t-\tau) + \alpha N^* \delta h_i(t-\tau) \\ & + \beta\,\delta v_{i+1}(t-\tau)\,, \end{aligned} \tag{4}$$

for $i = 2, \dots, N-1$. Here $N^* = V'(h^*)$ is the derivative of the range policy (2) at the equilibrium and the corresponding time headway is $t_{\rm h} = 1/N^*$.

Let us introduce the notation

$$x(t) = \delta v_i(t), \quad u_1(t) = \delta h_i(t), \quad u_2(t) = \delta v_{i+1}(t)\,. \tag{5}$$

Based on the dynamics (4) of vehicle i, we write out the parametric model

$$\dot{x} = a x(t-\tau) + b_1 u_1(t-\tau) + b_2 u_2(t-\tau)\,, \tag{6}$$

where the delay time τ and the feedback gains

$$a = -\alpha - \beta, \quad b_1 = \alpha N^*, \quad b_2 = \beta \tag{7}$$

are unknown a priori and to be determined through parameter identification.

III. Simultaneous Estimation of Gains and Delay

A. Direct Lyapunov method of approximated delay

This method was originally proposed in [10]. It bypasses the estimation of delay time by introducing multiple fictitious delays whose corresponding gains are zero, i.e., the parametric model (6) is rewritten as

$$\dot{x} = \sum_{i=1}^{n} \big(a_i x(t-\tau_i) + b_{1i} u_1(t-\tau_i) + b_{2i} u_2(t-\tau_i)\big)\,, \tag{8}$$

where $0 \le \tau_1 < \tau_2 < \cdots < \tau_n$, and there exists $j \in \{1, \dots, n\}$ such that the real delay $\tau = \tau_j$. Thus,

$$a_j = -\alpha - \beta, \quad b_{1j} = \alpha N^*, \quad b_{2j} = \beta\,, \tag{9}$$

and

$$a_i = b_{1i} = b_{2i} = 0\,, \tag{10}$$

for $i \ne j$. Then by identifying the zero gains we are able to "weed out" the "fake" delays and obtain the real delay time and corresponding feedback gains. Based on [10], the estimation algorithm for (8) is given by

$$\begin{aligned} \dot{\hat{x}}(t) =\ & \sum_{i=1}^{n} \big(\tilde{a}_i x(t-\tau_i) + \tilde{b}_{1i} u_1(t-\tau_i) + \tilde{b}_{2i} u_2(t-\tau_i)\big) \\ & + c\hat{x}(t)\,, \\ \dot{\tilde{a}}_i(t) =\ & \gamma_{0i}\hat{x}(t) x(t-\tau_i)\,, \\ \dot{\tilde{b}}_{1i}(t) =\ & \gamma_{1i}\hat{x}(t) u_1(t-\tau_i)\,, \\ \dot{\tilde{b}}_{2i}(t) =\ & \gamma_{2i}\hat{x}(t) u_2(t-\tau_i)\,, \end{aligned} \tag{11}$$

where tildes are used to denote estimated state and parameters, the state error is $\hat{x} = x - \tilde{x}$, and the estimation gains are $c > 0$, $\gamma_{ki} > 0$, $k = 0, 1, 2$, $i = 1, \dots, n$.

Define the vectors

$$Z = \begin{bmatrix} \hat{x} \\ \hat{A} \\ \hat{B}_1 \\ \hat{B}_2 \end{bmatrix}, \quad \hat{A} = \begin{bmatrix} \hat{a}_1 \\ \vdots \\ \hat{a}_n \end{bmatrix}, \quad \hat{B}_k = \begin{bmatrix} \hat{b}_{k1} \\ \vdots \\ \hat{b}_{kn} \end{bmatrix}, \tag{12}$$

that contain the estimation errors $\hat{a}_i = \tilde{a}_i - a_i$, $\hat{b}_{ki} = \tilde{b}_{ki} - b_{ki}$, $k = 1, 2$, $i = 1, \ldots, n$. Using (8,11), we can write the estimation model as a linear time-varying system:

$$\dot{Z} = \begin{bmatrix} -c & X_\tau^{\mathrm{T}} & U_{1\tau}^{\mathrm{T}} & U_{2\tau}^{\mathrm{T}} \\ \Gamma_0 X_\tau & 0 & 0 & 0 \\ \Gamma_1 U_{1\tau} & 0 & 0 & 0 \\ \Gamma_2 U_{2\tau} & 0 & 0 & 0 \end{bmatrix} Z\,, \tag{13}$$

where

$$\begin{aligned} &\Gamma_k = \operatorname{diag}\begin{bmatrix} \gamma_{k1} & \cdots & \gamma_{kn} \end{bmatrix}, \quad k = 0, 1, 2\,, \\ &X_\tau(t) = \begin{bmatrix} x(t-\tau_1) & \cdots & x(t-\tau_n) \end{bmatrix}^{\mathrm{T}}, \\ &U_{1\tau}(t) = \begin{bmatrix} u_1(t-\tau_1) & \cdots & u_1(t-\tau_n) \end{bmatrix}^{\mathrm{T}}, \\ &U_{2\tau}(t) = \begin{bmatrix} u_2(t-\tau_1) & \cdots & u_2(t-\tau_n) \end{bmatrix}^{\mathrm{T}}. \end{aligned} \tag{14}$$

We would like the fixed point $Z(t) \equiv 0$ of (13) to be (at least) Lyapunov stable. Thus, we define the Lyapunov function candidate

$$\begin{aligned} V &= \frac{1}{2} Z^{\mathrm{T}} \begin{bmatrix} 1 & & & \\ & \Gamma_0 & & \\ & & \Gamma_1 & \\ & & & \Gamma_2 \end{bmatrix}^{-1} Z \\ &= \frac{1}{2}\hat{x}^2 + \sum_{i=1}^{n} \frac{1}{2}\Big(\frac{1}{\gamma_{0i}}\hat{a}_i^2 + \frac{1}{\gamma_{1i}}\hat{b}_{1i}^2 + \frac{1}{\gamma_{2i}}\hat{b}_{2i}^2\Big)\,, \end{aligned} \tag{15}$$

and using (13), the Lie derivative becomes

$$\dot{V} = -c\hat{x}^2\,. \tag{16}$$

Since (15) is positive definite and (16) is negative semi-definite, $Z(t) \equiv 0$ is stable in the sense of Lyapunov, and the system (13) converges to the manifold of $\hat{x}(t) \equiv 0$ asymptotically.

On the other hand, the convergence of the estimated parameters ($\lim_{t\to\infty} \hat{A}(t) = 0, \lim_{t\to\infty} \hat{B}_1(t) = 0, \lim_{t\to\infty} \hat{B}_2(t) = 0$) results from the convergence of $\hat{x}$ given sufficiently rich signals $x(t), u_1(t), u_2(t)$, i.e., the persistent excitation condition. Here this condition requires piecewise continuous signals with a sufficient number of discontinuities at non-commensurable points [10], and in each continuous subinterval it also requires a sufficient number of Fourier components. Such "jumps" may be common in electronic signals, but they are seldom observed in mechanical systems such as the velocity of a car. Thus, it may not be easy to implement this method to estimate the parameters of a car-following model.

We also note that to obtain a more accurate estimation on the actual delay time τ, finer meshes of fictitious delay τ_i are required, which increases the dimension of the adaptive law (11). This would not only require more computational power, but also significantly slow down the convergence rate. If the identification becomes slower than the variation of driver behavior this method would eventually fail.

B. Method of state-dependent delay

To obtain a more accurate estimation of the delay time without relying on a high-dimensional parametric model, we consider an adaptive law where both the delay time and the feedback gains in (6) are identified simultaneously. In particular, we propose

$$\begin{aligned} \dot{\tilde{x}} &= \tilde{a}x(t-\tilde{\tau}) + \tilde{b}_1 u_1(t-\tilde{\tau}) + \tilde{b}_2 u_2(t-\tilde{\tau}) + c\hat{x}\,, \\ \dot{\tilde{a}} &= \gamma_1 \hat{x} x(t-\tilde{\tau})\,, \\ \dot{\tilde{b}}_1 &= \gamma_2 \hat{x} u_1(t-\tilde{\tau})\,, \\ \dot{\tilde{b}}_2 &= \gamma_3 \hat{x} u_2(t-\tilde{\tau})\,, \\ \dot{\tilde{\tau}} &= -\gamma_4 \hat{x}\tilde{\zeta}\,, \end{aligned} \tag{17}$$

where we use tildes to denote estimated state and parameters, the state error is defined as $\hat{x} = x - \tilde{x}$, and

$$\tilde{\zeta} = \tilde{a}\dot{x}(t-\tilde{\tau}) + \tilde{b}_1 \dot{u}_1(t-\tilde{\tau}) + \tilde{b}_2 \dot{u}_2(t-\tilde{\tau})\,. \tag{18}$$

Due to the adaptive law of $\tilde{\tau}$, (17) is a nonlinear system with state-dependent delay. To discuss the convergence of the algorithm, we denote the parameter errors by

$$\hat{a} = \tilde{a} - a, \quad \hat{b}_1 = \tilde{b}_1 - b_1, \quad \hat{b}_2 = \tilde{b}_2 - b_2, \quad \hat{\tau} = \tilde{\tau} - \tau\,, \tag{19}$$

and formulate the dynamics of $\hat{x}$ using (6,17)

$$\begin{aligned} \dot{\hat{x}} &= -c\hat{x}(t) + ax(t-\tau) - \tilde{a}x(t-\tilde{\tau}) \\ &\quad + b_1 u_1(t-\tau) - \tilde{b}_1 u_1(t-\tilde{\tau}) + b_2 u_2(t-\tau) - \tilde{b}_2 u_2(t-\tilde{\tau}) \\ &= -c\hat{x}(t) - \hat{a}x(t-\tau) - \hat{b}_1 u_1(t-\tau) - \hat{b}_2 u_2(t-\tau) \\ &\quad + \tilde{a}(x(t-\tau) - x(t-\tilde{\tau})) + \tilde{b}_1(u_1(t-\tau) - u_1(t-\tilde{\tau})) \\ &\quad + \tilde{b}_2(u_2(t-\tau) - u_2(t-\tilde{\tau}))\,. \end{aligned} \tag{20}$$

Assuming constant feedback gains in the parametric model (6) we obtain

$$\dot{\hat{a}} = \dot{\tilde{a}}\,, \quad \dot{\hat{b}}_1 = \dot{\tilde{b}}_1\,, \quad \dot{\hat{b}}_2 = \dot{\tilde{b}}_2\,, \quad \dot{\hat{\tau}} = \dot{\tilde{\tau}}\,. \tag{21}$$

While the convergence of approximated delay method (11) can be proven with negative semi-definiteness of the Lie derivative of a quadratic Lyapunov function (16), here we could not establish the negative semi-definiteness directly using similar quadratic Lyapunov functions, due to the estimated delay $\tilde{\tau}$. Thus we resort to the indirect Lyapunov method by first isolating the nonlinearity due to the time-varying delay $\tilde{\tau}$ and establishing convergence for the linearized dynamics.

We assume $x(t)$, $u_1(t)$ and $u_2(t)$ are bounded and have bounded derivatives up to the third order, and perform Taylor expansion to extract $\hat{\tau}$ from terms with time-varying delay

$$\begin{aligned} x(t-\tau) - x(t-\tilde{\tau}) &= \hat{\tau}\dot{x}(t-\tau) - \frac{1}{2}\hat{\tau}^2\ddot{x}(t-\tau) + \mathcal{O}(3)\,, \\ u_1(t-\tau) - u_1(t-\tilde{\tau}) &= \hat{\tau}\dot{u}_1(t-\tau) - \frac{1}{2}\hat{\tau}^2\ddot{u}_1(t-\tau) + \mathcal{O}(3)\,, \\ u_2(t-\tau) - u_2(t-\tilde{\tau}) &= \hat{\tau}\dot{u}_2(t-\tau) - \frac{1}{2}\hat{\tau}^2\ddot{u}_2(t-\tau) + \mathcal{O}(3)\,, \end{aligned} \tag{22}$$

where $\mathcal{O}(n)$ denotes n-th order terms in the state error $\hat{x}$ and the parameter errors $\hat{a}, \hat{b}_1, \hat{b}_2, \hat{\tau}$. Assuming constant gains and delay time in the parametric model (6), we have

$$\ddot{x}(t) = a\dot{x}(t-\tau) + b_1\dot{u}_1(t-\tau) + b_2\dot{u}_2(t-\tau)\,, \tag{23}$$

and (20) is rewritten as

$$\begin{aligned}\dot{\hat{x}} = &-c\hat{x}(t) - x(t-\tau)\hat{a} - u_1(t-\tau)\hat{b}_1 - u_2(t-\tau)\hat{b}_2 \\ &+ \ddot{x}(t)\hat{\tau} + g_0(\hat{a}, \hat{b}_1, \hat{b}_2, \hat{\tau})\,,\end{aligned} \tag{24}$$

where the higher-order terms are given by

$$\begin{aligned}g_0 = &\dot{x}(t-\tau)\hat{a}\hat{\tau} + \dot{u}_1(t-\tau)\hat{b}_1\hat{\tau} + \dot{u}_2(t-\tau)\hat{b}_2\hat{\tau} \\ &- \frac{\dddot{x}(t)}{2}\hat{\tau}^2 + \mathcal{O}(3).\end{aligned} \tag{25}$$

Similarly, we rewrite (17,21) as

$$\begin{aligned}\dot{\hat{a}} &= \gamma_1 x(t-\tau)\hat{x}(t) + g_1(\hat{x}, \hat{\tau})\,, \\ \dot{\hat{b}}_1 &= \gamma_2 u_1(t-\tau)\hat{x}(t) + g_2(\hat{x}, \hat{\tau})\,, \\ \dot{\hat{b}}_2 &= \gamma_3 u_2(t-\tau)\hat{x}(t) + g_3(\hat{x}, \hat{\tau})\,, \\ \dot{\hat{\tau}} &= -\gamma_4\ddot{x}(t)\hat{x}(t) + g_4(\hat{x}, \hat{a}, \hat{b}_1, \hat{b}_2, \hat{\tau})\,,\end{aligned} \tag{26}$$

where the higher-order terms are

$$\begin{aligned}g_1 &= -\gamma_1\dot{x}(t-\tau)\hat{x}\hat{\tau} + \mathcal{O}(3)\,, \\ g_2 &= -\gamma_2\dot{u}_1(t-\tau)\hat{x}\hat{\tau} + \mathcal{O}(3)\,, \\ g_3 &= -\gamma_3\dot{u}_2(t-\tau)\hat{x}\hat{\tau} + \mathcal{O}(3)\,, \\ g_4 &= -\gamma_4\big(\dot{x}(t-\tau)\hat{a} + \dot{u}_1(t-\tau)\hat{b}_1 + \dot{u}_2(t-\tau)\hat{b}_2 - \dddot{x}\hat{\tau}\big)\hat{x} \\ &\quad + \mathcal{O}(3).\end{aligned} \tag{27}$$

We define the state variable $Y = \begin{bmatrix}\hat{x} & \hat{a} & \hat{b}_1 & \hat{b}_2 & \hat{\tau}\end{bmatrix}^{\mathrm{T}}$ and then write (24,26) into state space form

$$\dot{Y} = \mathbf{M}(t)Y + \mathbf{N}(Y, t)\,, \tag{28}$$

where the coefficient matrix is given by

$$\begin{aligned}\mathbf{M}(t) &= \begin{bmatrix}-c & -v(t) \\ \Gamma v^{\mathrm{T}}(t) & 0\end{bmatrix}\,, \\ \Gamma &= \mathrm{diag}\begin{bmatrix}\gamma_1 & \gamma_2 & \gamma_3 & \gamma_4\end{bmatrix}\,, \\ v(t) &= \begin{bmatrix}x(t-\tau) & u_1(t-\tau) & u_2(t-\tau) & -\ddot{x}(t)\end{bmatrix}\,,\end{aligned} \tag{29}$$

and the higher-order terms are collected in

$$\mathbf{N}(Y, t) = \begin{bmatrix}g_0 & g_1 & g_2 & g_3 & g_4\end{bmatrix}^{\mathrm{T}}\,. \tag{30}$$

When the fixed point $Y(t) \equiv 0$ of (28) is uniformly asymptotically stable, both the state error $\hat{x}$ and the parameter errors $\hat{a}, \hat{b}_1, \hat{b}_2, \hat{\tau}$ are guaranteed to decay to zero. It has been found that given $c > 0$, the uniform asymptotic stability of $\dot{Y} = \mathbf{M}(t)Y$ is equivalent to the persistent excitation condition of the signal $v(t)$ [15]. That is, there exists positive constants T_0, δ_0, and ϵ_0 such that for all $t_1 \geq 0$ and a unit vector w with the same dimension as $v(t)$, there is a $t_2 \in [t_1, t_1 + T_0]$ such that

$$\Big|\int_{t_2}^{t_2+\delta_0} v(\theta)w^{\mathrm{T}}\mathrm{d}\theta\Big| \geq \epsilon_0\,. \tag{31}$$

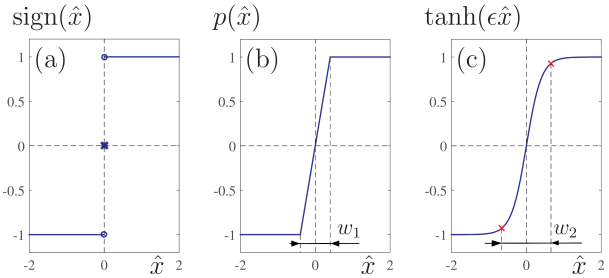

Fig. 2. (a): The non-continuous sign function (33).(b): The non-smooth piecewise linear function (34) with the width of boundary layer $w_1 = 2\epsilon$. (c): The infinitely smooth hyperbolic tangent function (35) with the width of boundary layer $w_2 = \epsilon\ln(2+\sqrt{3})$. We set $\epsilon = 0.4$ in (b,c).

This establishes the local convergence of this algorithm.

However, the size of the basin of attraction depends on the nonlinear term $\mathbf{N}(Y, t)$. While we assume the input signals $x(t), u_1(t), u_2(t)$ are bounded, the bounds in general depend on the magnitude of different frequency components in $u_2(t)$. These bounds, together with the choice of adaptation gains $\gamma_1, \gamma_2, \gamma_3, \gamma_4$, determine the basin of attraction. We believe that the size of the basin of attraction can be estimated through bifurcation analysis. Here, due to page limit, we only point out that the algorithm is observed to perform well even for initial guesses with relatively large parameter errors, when considering properly chosen adaptation gains and sufficiently rich signals based on experiences from parameter estimation in non-delayed systems.

Meanwhile, having an adaptive law for the delay time instead of a grid approximation has been found to be important to ensure the performance of the parameter estimation. Consequently, this method is more practical for applications like connected vehicle systems.

C. Modified method of state-dependent delay

It is noted in sliding mode control that the switching between different control laws in different regions of the state space may increase the convergence rate [16]. Motivated by the estimator proposed in [11], we consider introducing the sign function into our adaptive law and rewrite it as

$$\begin{aligned}\dot{\hat{x}} &= \tilde{a}x(t-\tilde{\tau}) + \tilde{b}_1u_1(t-\tilde{\tau}) + \tilde{b}_2u_2(t-\tilde{\tau}) + c\hat{x}\,, \\ \dot{\tilde{a}} &= \gamma_1 f(\hat{x})x(t-\tilde{\tau})\,, \\ \dot{\tilde{b}}_1 &= \gamma_2 f(\hat{x})u_1(t-\tilde{\tau})\,, \\ \dot{\tilde{b}}_2 &= \gamma_3 f(\hat{x})u_2(t-\tilde{\tau})\,, \\ \dot{\tilde{\tau}} &= -\gamma_4 f(\hat{x})\tilde{\zeta}\,,\end{aligned} \tag{32}$$

where $\tilde{\zeta}$ is given by (18) and we may use the switching function

$$f(\hat{x}) = \mathrm{sign}(\hat{x}) = \begin{cases}-1 & \text{if} \quad \hat{x} < 0\,, \\ 0 & \text{if} \quad \hat{x} = 0\,, \\ 1 & \text{if} \quad \hat{x} > 0\,,\end{cases} \tag{33}$$

that is plotted in Fig. 2(a).

However, the sign function cannot be perfectly implemented numerically, which typically leads to high-frequency

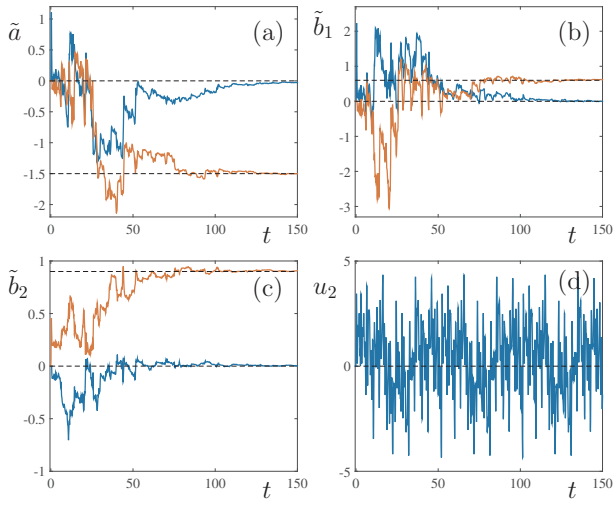

Fig. 3. (a,b,c): Estimated feedback gains using (11). The blue curves are gains corresponding to $\tau_1 = 0$ [s], and the red curves corresponds to $\tau_2 = 0.5$ [s]. The dashed lines mark the real value of a, b_1, and b_2, respectively. (d): The input signal $u_2(t) = \delta v_{i+1}(t)$ used by the estimator (8) is discontinuous at $t \approx 2.7, 52.1, 101.5$ [s]. In each continuous subinterval $u_2(t) = \sum_{j=1}^{6} \sin(\omega_j t + \rho_j)$ with frequency components $\omega_j \in \{0.2, 0.6, 1.5, 3.8, 5.3, 7\}$ [rad/s].

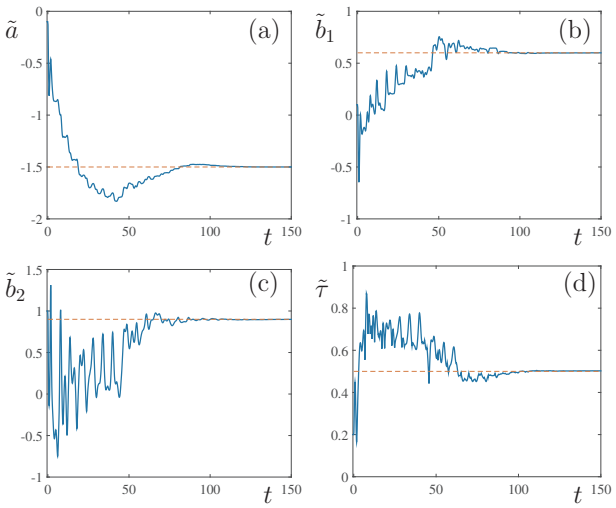

Fig. 4. Estimated feedback gains and delay time using the estimator (17). The dashed lines mark the real parameter values. The signals are generated using (4,5) with $u_2(t) = \delta v_{i+1}(t) = \frac{2}{3}\big(\cos(t) + \cos(2.1t) + \cos(7t)\big)$. The estimator gains are $\gamma_1 = 1.5$, $\gamma_2 = 1.5$, $\gamma_3 = 6.0$, $\gamma_4 = 1.0$.

oscillation (called chattering) in the vicinity of the sliding surface. To eliminate chattering, we define a boundary layer $|\hat{x}| \le \epsilon$, $\epsilon > 0$ and define the switching function as

$$f(\hat{x}) = p(\hat{x}) = \begin{cases} 1 & \text{if} \quad \hat{x} > \epsilon\,, \\ \hat{x}/\epsilon & \text{if} \quad -\epsilon \le \hat{x} \le \epsilon\,, \\ -1 & \text{if} \quad \hat{x} < -\epsilon\,, \end{cases} \tag{34}$$

as shown in Fig. 2(b). Here ϵ is used to adjust the gradient of the switching function, and consequently the width $w_1 = 2\epsilon$ of the boundary layer. Note that inside the boundary layer, (34) is linear and the estimator (32,34) is equivalent to (17).

In order to avoid non-smoothness when entering the boundary layer, we may use a hyperbolic tangent function

$$f(\hat{x}) = \tanh\big(\hat{x}/\epsilon\big)\,, \tag{35}$$

as shown in Fig. 2(c). Again, ϵ determines the gradient, and by calculating the third-order inflection points ($\partial^3_{\hat{x}} \tanh\big(\hat{x}/\epsilon\big) = 0$) we obtain the width of the boundary layer as $w_2 = \epsilon \ln(2+\sqrt{3})$. Indeed, as ϵ decreases, the width of both boundary layers in (34) and (35) tend to zero, and (34) and (35) converges to (33).

We note that when implementing algorithms that contain the dynamics of $\tilde{\tau}$, a lower bound and an upper bound on the estimation $\tilde{\tau}$ are needed. In this paper, we set $\tilde{\tau} \in [0, \tau_{\max}]$, where $\tau_{\max}$ is the maximum delay time known a priori.

IV. Simulations

In this section, we implement the method of approximated delay (11), and the original and modified methods of state-dependent delay (17,32) to estimate the delay time and feedback gains in the parametric car-following model (6), and compare their performances.

We use $v_{\max} = 30$ [m/s], $h_{\rm st} = 5$ [m], $h_{\rm go} = 35$ [m] that corresponds to realistic traffic data [13] in the range policy (2), which results in the constant slope $N^* = 1$ [1/s] corresponding to the constant time headway $t_{\rm h} = 1/N^* = 1$ [s]. Moreover, we set the equilibrium at $(h^*, v^*) = (20\,[\rm m], 15\,[\rm m/s])$ and use the gains $\alpha = 0.6$ [1/s], $\beta = 0.9$ [1/s] and reaction time $\tau = 0.5$ [s]. Then the real parameter values in the parametric model (6) are $a = -1.5$ [1/s], $b_1 = 0.6$ [1/s], $b_2 = 0.9$ [1/s]; see (7).

For the first method (11), we assume one fictitious delay time $\tau_1 = 0$ [s] aside from the real delay time $\tau_2 = 0.5$ [s]. The signals $x(t)$, $u_1(t)$, $u_2(t)$ are generated by the linearized car-following model (4,5) with non-smooth velocity perturbation $u_2(t)$ with frequency components $\omega_j \in \{0.2, 0.6, 1.5, 3.8, 5.3, 7\}$ [rad/s]. The trajectory of estimated parameters are shown in Fig. 3(a,b,c). Note that while the parameters converge within 150 [s], the velocity profile of vehicle $i+1$ contains 6 frequency components and 3 discontinuities to meet the persistent excitation condition (see the caption of Fig. 3). Such non-smooth velocity profile is not commonly observed in cars on road, as vehicles can be viewed as low-pass filters. Thus, the convergence rate of this estimator may be significantly slower in real-world implementation. Also, the number of estimated parameters ($3n$) increases with the number of fictitious delays (n), leading to observed deterioration of convergence rate in simulations. Meanwhile, as the mesh for delay time becomes finer, the time interval between mesh points shortens. As a result, the numerical algorithm will have increasing difficulty in correctly identifying gains corresponding to each mesh point. Thus, it is difficult to preserve the convergence rate in Fig. 3 when we do not start with the exact guess of $\tau_2 = 0.5$ [s].

Fig. 4 and Fig. 5 show the performance of the estimators (17) and (32,35), respectively. Signals $x(t)$, $u_1(t)$, $u_2(t)$ are generated by the linearized car-following model (4,5) with

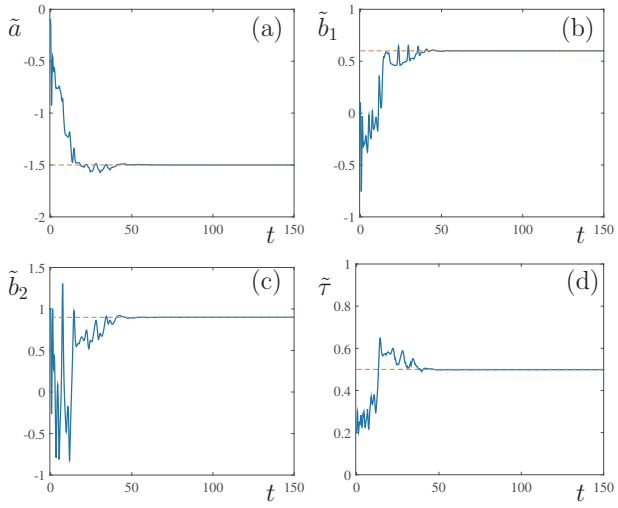

Fig. 5. Estimated feedback gains and delay time using the estimator (32,35). The notations and input signals are the same as in Fig. 4. The estimator gains are $\gamma_1 = 1.5$, $\gamma_2 = 1.5$, $\gamma_3 = 4.0$, $\gamma_4 = 0.35$, and we set $\epsilon = 0.4$.

a sinusoidal velocity perturbation $u_2(t) = \delta v_{i+1}(t) = \frac{2}{3}\big(\cos(t)+\cos(2.1t)+\cos(7t)\big)$. In both figures, the feedback gains and delay converge to the real values within reasonable amount of time, producing more accurate estimations than in Fig. 3. However, the convergence rate is faster in Fig. 5, which illustrates the potential benefits of the modified estimator (32,35).

V. Conclusion

We performed parameter estimation for car-following models with driver reaction time using three different estimators. First, we investigated the method of multiple delays, which is a direct extension of parameter estimation in systems without delay. However, it required non-continuous signals for persistent excitation and the convergence rate deteriorated rapidly as the number of fictitious delays were increased. Then we proposed the method of state-dependent delay, which is able to provide accurate estimation of delay time and feedback gains, without sacrificing the convergence rate. Finally, we improved the second method by introducing switching behaviors using the sign function and its smooth approximations, and demonstrated the improvement of the convergence rate. We conclude that the latter two methods are suitable for applications in connected vehicle design, and future research may include the robustness and global stability analysis of the adaptive laws as nonlinear systems with state-dependent delays.

References

[1] P. Seiler, A. Pant, and K. Hedrick, "Disturbance propagation in vehicle strings," *Automatic Control, IEEE Transactions on*, vol. 49, no. 10, pp. 1835–1842, 2004.

[2] G. Orosz, "Connected cruise control: modeling, delay effects, and nonlinear behavior," *Vehicle System Dynamics*, p. submitted, 2014.

[3] L. Zhang and G. Orosz, "Designing network motifs in connected vehicle systems: delay effects and stability," in *Proceedings of the ASME Dynamical Systems and Control Conference*. ASME, 2013, p. V003T42A006, paper no. DSCC2014-6358.

[4] W. B. Qin, M. M. Gomez, and G. Orosz, "Stability and frequency response under stochastic communication delays with applications to connected cruise control design," *IEEE Transactions on Intelligent Transportation Systems*, p. submitted, 2015.

[5] R. Pandita and D. Caveney, "Preceding vehicle state prediction," in *2013 IEEE Intelligent Vehicles Symposium*, 2013, pp. 1000–1006.

[6] J. I. Ge and G. Orosz, "Dynamics of connected vehicle systems with delayed acceleration feedback," *Transportation Research Part C*, vol. 46, pp. 46–64, 2014.

[7] P. A. Ioannou and J. Sun, *Robust Adaptive Control*. Dover Publications, 2012.

[8] S. Diop, I. Kolmanovsky, P. Moraal, and M. V. Nieuwstadt, "Preserving stability/performance when facing an unknown time-delay," *Control Engineering Practice*, vol. 9, no. 12, pp. 1319–1325, 2001.

[9] O. Gomez, Y. Orlov, and I. V. Kolmanovsky, "On-line identification of SISO linear time-invariant delay systems from output measurements," *Automatica*, vol. 43, no. 12, pp. 2060 – 2069, 2007.

[10] Y. Orlov, L. Belkoura, J.-P. Richard, and M. Dambrine, "Adaptive identification of linear time-delay systems," *International Journal of Robust and Nonlinear Control*, vol. 13, pp. 857–872, 2003.

[11] S. Drakunov, W. Perruquetti, J.-P. Richard, and L. Belkoura, "Delay identification in time-delay systems using variable structure observers," *Annual Reviews in Control*, vol. 30, no. 2, pp. 143–158, 2006.

[12] L. Zhang and G. Orosz, "Motif-based analysis of connected vehicle systems: delay effects and stability," *IEEE Transaction on Intelligent Transportation Systems*, p. accepted, 2015.

[13] G. Orosz, R. E. Wilson, and G. Stépán, "Traffic jams: dynamics and control," *Philosophical Transactions of the Royal Society A*, vol. 368, no. 1928, pp. 4455–4479, 2010.

[14] G. Orosz, J. Moehlis, and F. Bullo, "Delayed car-following dynamics for human and robotic drivers," in *Proceedings of the ASME IDETC/CIE Conference*. ASME, 2011, pp. 529–538, paper no. DETC2011-48829.

[15] A. P. Morgan and K. S. Narendra, "On the stability of nonautonomous differential equations $\dot{x} = [\mathbf{A} + \mathbf{B}(t)]x$ with skew symmetric matrix $\mathbf{B}(t)$," *SIAM Journal of Control and Optimization*, vol. 15, no. 1, pp. 163–175, 1977.

[16] J.-J. E. Slotine and W. Li, *Applied Nonlinear Control*. Prenice Hall, 1991.